proceedings

MDPI

Proceedings

Synthesis and Characterization of a Fullerenol Derivative for Potential Biological Applications †

Eduardo Ravelo-Nieto [1], Alvaro Duarte-Ruiz [1], Luis H. Reyes [2] and Juan C. Cruz [3,*]

[1] Department of Chemistry, Universidad Nacional de Colombia, Ciudad Universitaria, Cra. 30 No 45-03, Bogotá, Colombia; eravelo@unal.edu.co (E.R.-N.); aduarter@unal.edu.co (A.D.-R.)
[2] Department of Chemical Engineering, Universidad de Los Andes, Cra. 1E No. 19a-40, Bogotá, DC 111711, Colombia; lh.reyes@uniandes.edu.co
[3] Department of Biomedical Engineering, Universidad de Los Andes, Cra. 1E No. 19a-40, Bogotá, DC 111711, Colombia
* Correspondence: jc.cruz@uniandes.edu.co
† Presented at the 2nd International Online-Conference on Nanomaterials, 15–30 November 2020; Available online: https://iocn2020.sciforum.net/.

Published: 15 November 2020

Abstract: Several biological barriers are generally responsible for the limited delivery of cargoes at the cellular level. Fullerenols have unique structural features and possess suitable properties for interaction with the cells. This study aimed to synthesize and characterize a fullerenol derivative with desirable characteristics (size, charge, functionality) to develop cell penetration vehicles. Fullerenol was synthesized from fullerene C_{60} solubilized in toluene followed by hydroxylation with hydrogen peroxide and tetra-n-butylammonium hydroxide (TBAH) as a phase transfer catalyst. The obtained product was purified by a Florisil chromatography column (water as the eluent) followed by dialysis (cellulose membrane dialysis tubing) and freeze-drying (yield 66%). Subsequently, a silane coupling agent was conjugated on the fullerenol surface to render free amine functional groups for further covalent functionalization with other molecules. Characterization via UV-visible, FTIR-ATR, Raman, DLS, and SEM techniques was conducted to evaluate composition, size, morphology, surface functionality, and structural properties. We are currently working on the conjugation of the potent cell-penetrating agents Buforin II (BUFII) and the Outer Membrane Protein A (OmpA) on the surface of the fullerenol to estimate whether cell penetration and endosome escape are improved concerning conventional polymeric vehicles and our previous developments with Iron Oxide Nanoparticles.

Keywords: fullerenol; cell-penetrating agent; Buforin II; OmpA

1. Introduction

The nanocarriers' design for pharmaceutical applications one of the main challenges is to overcome several biological barriers as they are generally responsible for the limited delivery of functional cargoes at the target sites. The main consequence is the limited bioavailability of the pharmacological molecules, which is reflected in an increased number of dosages to reach the minimum effective concentration [1,2]. At the cellular scale, some of these barriers include the plasma membrane for the initial internalization and the endosomal one after cellular uptake. Moreover, for applications in gene delivery, the nanocarriers might need to come across the nuclear envelope [3,4]. One attractive strategy to address this challenge is the surface engineering of the nanocarriers with chemical functionalities that provide specific interactions with the constituents of the biological barriers to penetrate and eventually pass them [3–7]. Among many others, some of the molecules for functionalization include natural and synthetic polymers, translocating proteins and peptides,

phospholipids, and polysaccharides [3,8,9]. Depending on various physicochemical parameters of the nanoplatform (e.g., size, surface chemistry, charge, topology), the interactions with such molecules might vary significantly and alter their functionality [3,10,11]. As a result, the same molecule conjugated to different nanoplatforms might exhibit different interactions with subcellular compartments [12]. Over the past three years, we developed a new family of nanobioconjugates with cell-penetrating abilities and endosomal escape by immobilizing the antimicrobial peptide BUF-II and the biosurfactant protein OmpA on Iron Oxide nanoparticles [13–15]. We are currently exploring the impact of changing the nanostructured support on the translocating abilities and intracellular trafficking of the obtained nanobioconjugates. Accordingly, here we propose that the fullerenol derivatives may provide a suitable immobilization support for translocating molecules mainly due to their structural features, hydrophilic properties, and hollow spherical shape [6,16]. This work was therefore aimed at obtaining a fullerenol derivative with features that allow these potent cell-penetrating agents' conjugation.

2. Materials and Methods

2.1. Materials

Fullerene C_{60} was purchased from Frontier Carbon Corporation. Tetra-n-butylammonium hydroxide (TBAH) (40% in water), tetramethylammonium hydroxide (TMAH) (25%), (3-Aminopropyl) triethoxysilane (APTES) (98%), and acetic acid glacial were purchased from Sigma-Aldrich. Hydrogen peroxide (H_2O_2) solution 32% was purchased from Merck (Darmstadt, Germany).

2.2. Synthesis and Silanization of Fullerenol

Our fullerenol product was first prepared with a modification to a previously reported method [17]. To a solution of fullerene C_{60} (100 mg) in toluene (50 mL), an aqueous solution of 30% hydrogen peroxide (10 mL) and tetra-n-butylammonium hydroxide, TBAH (40% in water, 500 μL) was added and stirred for 16 h at 60 °C. Subsequently, the aqueous phase was separated from the organic phase, and to eliminate residual TBAH, the aqueous phase containing the fullerenol was passed through a chromatographic column using Florisil as an absorbent and type II water as eluent. Then, to complete the purification, we combined dialysis (cellulose membrane dialysis tubing) and freeze-drying (Yield 66%) [18]. Next, 50 mg of fullerenol was dissolved in 15 mL of type II water. TMAH solution (500 μL, 25% (*v*/*v*)) and 25 μL of glacial acetic acid were then added to the solution and sonicated 10 min. APTES solution (500 μL, 20% (*v*/*v*)) was added to the fullerenol solution for silanization. The silanized fullerenol was washed with type II water to remove the excess of APTES [19]. Figure 1 shows a schematic of the synthesis procedure.

2.3. Fullerenol and Fullerenol Derivative Characterization

UV–visible spectra were recorded with a GENESYS 10S UV-vis spectrophotometer (Thermo Fisher Scientific Inc., Massachusetts, USA). Infrared (FTIR) spectra were recorded with a Bruker Alpha II FTIR Eco-ATR (Bruker Optik GmbH, Ettlingen, Germany). Spectra were collected in the range of 4000–400 cm^{-1} with a spectral resolution of 2 cm^{-1}. Raman spectroscopy data were collected with a DXR Raman microscope (Thermo Fisher Scientific) system by exciting with the 532 nm line of an Ar ion laser. The exciting power at the sample was 8 mW with typical exposure time of 24 s and at least 5 repetitions. The system is equipped with a 900 lines per millimeter holographic grating. Nanoparticle size was determined through Dynamic Light Scattering (DLS, Zeta-Sizer Nano-ZS; Malvern Instruments, Malvern, UK). Scanning Electron Microscopy (SEM) analysis of fullerenol was carried out in a TESCAN VEGA 3.

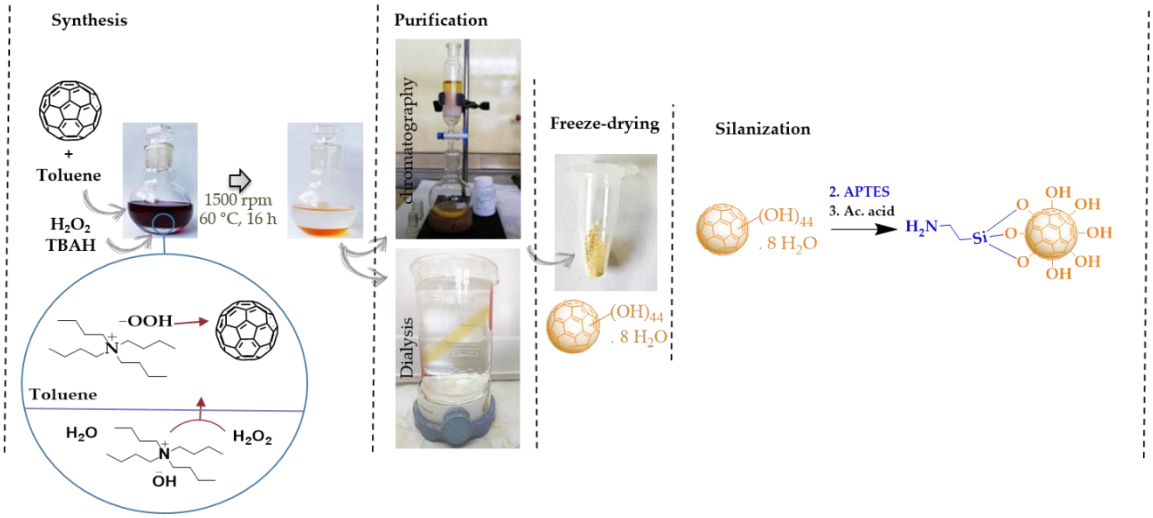

Figure 1. Synthesis and purification of fullerenol and fullerenol derivative. First, fullerene C_{60} was solubilized in toluene followed by hydroxylation with H_2O_2 and TBAH as a catalyst. The obtained product was purified by a Florisil chromatography column (water as the eluent) followed by dialysis (cellulose membrane dialysis tubing) and freeze-drying. Finally, the fullerenol was silanized with APTES to render free amine functional groups for further covalent functionalization with other molecules.

3. Results and Discussion

Since Fullerene C_{60} is insoluble in water, it was solubilized in toluene (purple coloration). After putting this solution in contact with the aqueous H_2O_2 solution, we observed two distinct liquid phases. TBAH is essential as it acts as a phase transfer catalyst by mediating the interaction between hydrophilic -OOH groups in the aqueous phase and the hydrophobic fullerenes in the organic phase. Once the reaction occurs, this organic phase becomes colorless and, upon standing still for 15 min, a yellow aqueous phase separates from the mixture (Figure 1) [8].

Fullerene C_{60} in toluene and fullerenol in water UV–visible absorption spectra are shown in Figure 2a. C_{60} fullerene dissolved in toluene has a purple coloration and characteristic absorption bands between 300 nm and 410 nm with a maximum at 283 nm, 335 nm, and 408 nm, followed by a broad absorption band in the range of 430 to 650 nm [20]. Fullerenol dissolved in water has a yellow coloration and is almost transparent in the visible region, due to its considerably decreased π-conjugation compare to fullerene C_{60}. Figure 2b shows the infrared spectra of C_{60} fullerene (precursor), unpurified fullerenol (with TBAH residues), purified fullerenol, and silanized fullerenol. Fullerene C_{60} has four characteristic infrared absorption bands of high intensity at 1429, 1182, 573, and 525 cm^{-1} due to C-C bonds (Figure 2b(1)) [21]. In the unpurified fullerenol, the two peaks observed at 2800–3000 cm^{-1} were attributed to residual TBAH (Figure 2b(2)). Purified fullerenol showed broadband at around 3383 cm^{-1} (O-H *stretching vibration, st*) and four characteristic bands at 1591 cm^{-1} (C=C *st*), 1403 cm^{-1} (O-H *deformation vibration, δ*), 1360 cm^{-1} (C-O-H *δ*), and 1108 cm^{-1} (C-O *st*), which agree well with previous reports (Figure 2b(3)). Silanization with APTES was confirmed by the presence of the new bands at 2944 cm^{-1} and 2854 cm^{-1} due to C-H asymmetrical and symmetrical stretching vibrations. Moreover, we identified the absorption bands at 1653 cm^{-1} (N-H *δ*), 1384 cm^{-1} (C-H), 1110 cm^{-1} (Si-O *st*), 1052 cm^{-1} (Si-O-Si *st*), and 690 cm^{-1} (Si-C *st*) which overlap with the absorption bands of fullerenol (Figure 2b(4)) [13]. The Raman spectrum of the purified fullerenol in Figure 2c shows characteristics bands between 1700–1000 cm^{-1}, which can be attributed to the C−C stretching vibrations [9]. However, the torsional motion of the C−O−H group is not visible. The fullerenols should have a diameter of ~1.0 nm but tend to aggregate easily, as seen in Figure 2d where the average hydrodynamic diameter approach 11 nm with a relatively narrow distribution [22–24]. SEM images of fullerenol in Figure 2e show flakes-like morphology similar to pristine fullerene as reported elsewhere [25,26].

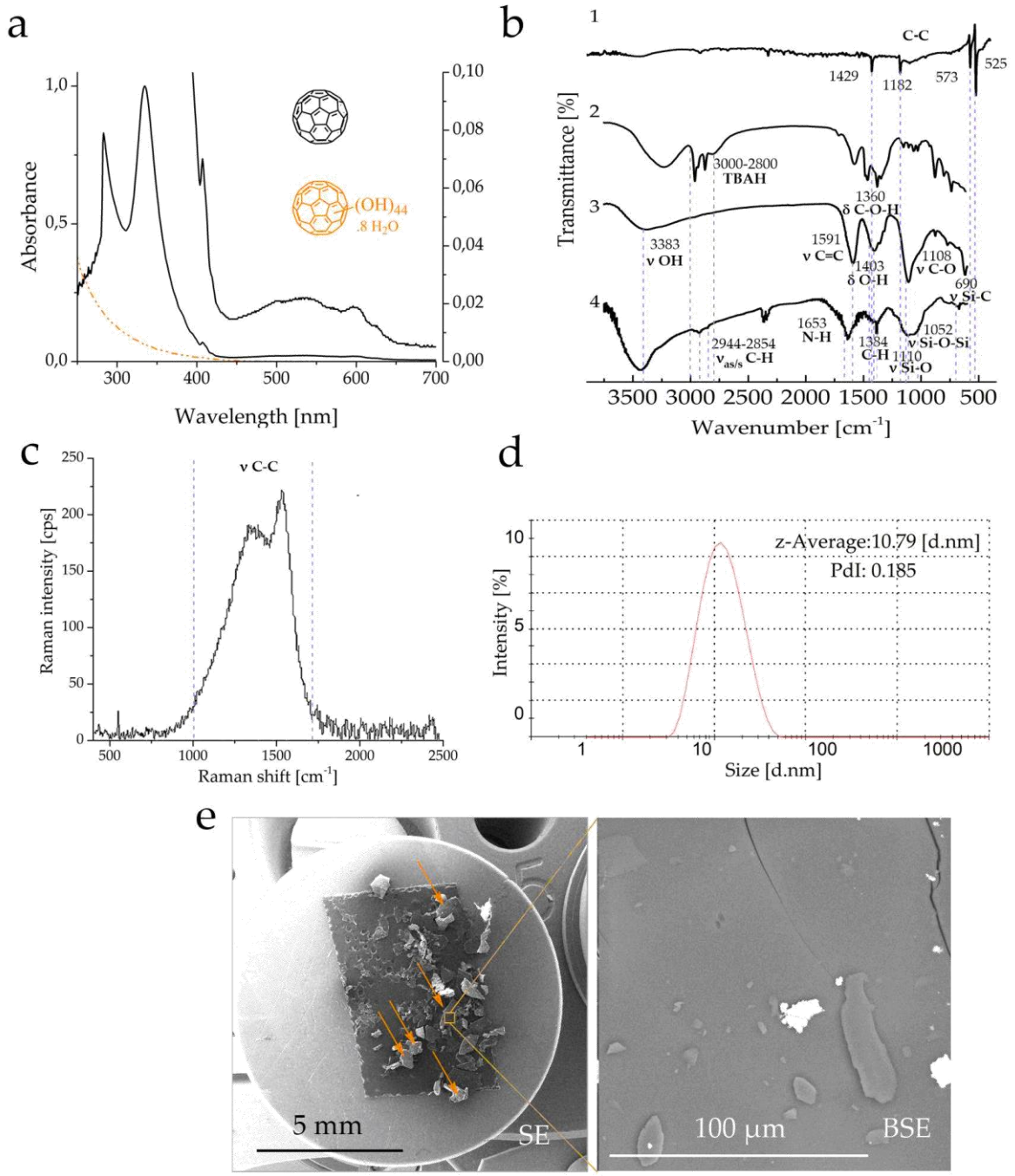

Figure 2. (**a**) UV-vis spectra of C_{60} in toluene and aqueous solution of fullerenol; (**b**) FTIR spectra of (1) fullerene, (2) fullerenol as produced, (3) purified fullerenol, (4) silanized fullerenol. (**c**) Raman spectrum purified fullerenol; (**d**) DLS histogram for the size intensity distribution; (**e**) SEM images of fullerenol, the orange arrows show flakes-like morphology (Left: MAG 17X, Det: SE, HV: 20.0 kV. Right: MAG 1.5kX, Det: BSE, HV: 20.0 kV).

4. Conclusions

This synthesis and purification methodology proposed here allowed us to obtain a fullerenol derivative with free amine groups on the surface, which can be potentially exploited to conjugate the protein OmpA or the peptide BUFII via either amide or imine bonds. We are currently working on these conjugations to estimate whether cell penetration and endosome escape are improved concerning conventional polymeric vehicles and our previous developments with Iron Oxide Nanoparticles.

Author Contributions: Conceptualization, J.C.C., A.D.-R. and L.H.R.; Methodology, data curation, and data analysis E.R.-N., J.C.C., A.D.-R. and L.H.R.; Formal analysis and investigation, E.R.-N.; Validation, J.C.C., A.D.-R. and L.H.R.; Writing—original draft preparation, E.R.-N.; Writing—review and editing, J.C.C., A.D.-R. and L.H.R.; Supervision, J.C.C., A.D.-R. and L.H.R. All authors have read and agreed to the published version of the manuscript.

Funding: This work was supported by Minciencias grant 689-2018.

Acknowledgments: The authors would like to thank the Department of Biomedical Engineering and Food and Chemical engineering for technical support.

References

1. Price, G.; Patel, D.A. Drug Bioavailability. Available online: https://www.ncbi.nlm.nih.gov/books/NBK557852/ (accessed on 10 November 2020).
2. Pramanik, A.; Garg, S. Design of diffusion-controlled drug delivery devices for controlled release of Paclitaxel. *Chem. Biol. Drug Des.* **2019**, *94*, 1478–1487, doi:10.1111/cbdd.13524.
3. Behzadi, S.; Serpooshan, V.; Tao, W.; Hamaly, M.A.; Alkawareek, M.Y.; Dreaden, E.C.; Brown, D.; Alkilany, A.M.; Farokhzad, O.C.; Mahmoudi, M. Cellular uptake of nanoparticles: Journey inside the cell. *Chem. Soc. Rev.* **2017**, *46*, 4218–4244, doi:10.1039/c6cs00636a.
4. Selby, L.I.; Cortez-Jugo, C.M.; Such, G.K.; Johnston, A.P.R. Nanoescapology: Progress toward understanding the endosomal escape of polymeric nanoparticles. *Wiley Interdiscip. Rev. Nanomed. Nanobiotechnology* **2017**, *9*, e1452, doi:10.1002/wnan.1452.
5. Saei, A.A.; Yazdani, M.; Lohse, S.E.; Bakhtiary, Z.; Serpooshan, V.; Ghavami, M.; Asadian, M.; Mashaghi, S.; Dreaden, E.C.; Mashaghi, A.; et al. Nanoparticle Surface Functionality Dictates Cellular and Systemic Toxicity. *Chem. Mater.* **2017**, *29*, 6578–6595, doi:10.1021/acs.chemmater.7b01979.
6. Kazemzadeh, H.; Mozafari, M. Fullerene-based delivery systems. *Drug Discov. Today* **2019**, *24*, 898–905, doi:10.1016/j.drudis.2019.01.013.
7. Mi, P.; Cabral, H.; Kataoka, K. Ligand-Installed Nanocarriers toward Precision Therapy. *Adv. Mater.* **2020**, *32*, e1902604, doi:10.1002/adma.201902604.
8. Smith, S.A.; Selby, L.I.; Johnston, A.P.R.; Such, G.K. The Endosomal Escape of Nanoparticles: Toward More Efficient Cellular Delivery. *Bioconjugate Chem.* **2019**, *30*, 263–272, doi:10.1021/acs.bioconjchem.8b00732.
9. Ahmad, A.; Khan, J.M.; Haque, S. Strategies in the design of endosomolytic agents for facilitating endosomal escape in nanoparticles. *Biochimie* **2019**, *160*, 61–75, doi:10.1016/j.biochi.2019.02.012.
10. Chakraborty, S.; Dhakshinamurthy, G.S.; Misra, S.K. Tailoring of physicochemical properties of nanocarriers for effective anti-cancer applications. *J. Biomed. Mater. Res. Part A* **2017**, *105*, 2906–2928, doi:10.1002/jbm.a.36141.
11. Biffi, S.; Voltan, R.; Bortot, B.; Zauli, G.; Secchiero, P. Actively targeted nanocarriers for drug delivery to cancer cells. *Expert Opin. Drug Deliv.* **2019**, *16*, 481–496, doi:10.1080/17425247.2019.1604679.
12. Kanwal, U.; Bukhari, N.I.; Ovais, M.; Abass, N.; Hussain, K.; Raza, A. Advances in nano-delivery systems for doxorubicin: An updated insight. *J. Drug Target.* **2018**, *26*, 296–310, doi:10.1080/1061186x.2017.1380655.
13. Cuellar, M.; Cifuentes, J.; Perez, J.; Suarez-Arnedo, A.; Serna, J.A.; Groot, H.; Muñoz-Camargo, C.; Cruz, J.C. Novel BUF2-magnetite nanobioconjugates with cell-penetrating abilities. *Int. J. Nanomed.* **2018**, *13*, 8087–8094, doi:10.2147/ijn.s188074.
14. Perez, J.; Cifuentes, J.; Cuellar, M.; Suarez-Arnedo, A.; Cruz, J.C.; Muñoz-Camargo, C. Cell-penetrating and antibacterial BUF-II nanobioconjugates: Enhanced potency via immobilization on polyetheramine-modified magnetite nanoparticles. *Int. J. Nanomed.* **2019**, *14*, 8483–8497, doi:10.2147/ijn.s224286.
15. Lopez-Barbosa, N.; Suárez-Arnedo, A.; Cifuentes, J.; Barrios, A.F.G.; Batista, C.A.S.; Osma, J.F.; Muñoz-Camargo, C.; Cruz, J.C. Magnetite–OmpA Nanobioconjugates as Cell-Penetrating Vehicles with Endosomal Escape Abilities. *ACS Biomater. Sci. Eng.* **2019**, *6*, 415–424, doi:10.1021/acsbiomaterials.9b01214.
16. Semenov, K.; Charykov, N.; Postnov, V.; Sharoyko, V.; Vorotyntsev, I.; Galagudza, M.; Murin, I.V. Fullerenols: Physicochemical properties and applications. *Prog. Solid State Chem.* **2016**, *44*, 59–74, doi:10.1016/j.progsolidstchem.2016.04.002.
17. Kokubo, K.; Shirakawa, S.; Kobayashi, N.; Aoshima, H.; Oshima, T. Facile and scalable synthesis of a highly hydroxylated water-soluble fullerenol as a single nanoparticle. *Nano Res.* **2011**, *4*, 204–215, doi:10.1007/s12274-010-0071-z.

18. De Santiago, H.A.; Gupta, S.K.; Mao, Y. On high purity fullerenol obtained by combined dialysis and freeze-drying method with its morphostructural transition and photoluminescence. *Sep. Purif. Technol.* **2019**, *210*, 927–934, doi:10.1016/j.seppur.2018.08.033.
19. Hermanson, G.T. Introduction to Bioconjugation. In *Bioconjugate Techniques*; Academic press: Cambridge, MA, USA, 2013; pp. 1–125.
20. Ajie, H.; Alvarez, M.M.; Anz, S.J.; Beck, R.D.; Diederich, F.; Fostiropoulos, K.; Huffman, D.R.; Kraetschmer, W.; Rubin, Y.; Schriver, K.E.; et al. Characterization of the soluble all-carbon molecules C60 and C70. *J. Phys. Chem.* **1990**, *94*, 8630–8633, doi:10.1021/j100387a004.
21. Kratschmer, W.; Lamb, L.D.; Fostiropoulos, K.; Huffman, D.R. Solid C60: A new form of carbon. *Nature* **1990**, *347*, 354–358, doi:10.1038/347354a0.
22. Kokubo, K.; Matsubayashi, K.; Tategaki, H.; Takada, H.; Oshima, T. Facile Synthesis of Highly Water-Soluble Fullerenes More Than Half-Covered by Hydroxyl Groups. *ACS Nano* **2008**, *2*, 327–333, doi:10.1021/nn700151z.
23. Kovač, T.; Borišev, I.; Crevar, B.; Kenjerić, F.Č.; Ko, M. Fullerol C60(OH)24 nanoparticles modulate aflatoxin B1 biosynthesis in Aspergillus flavus. *Sci. Rep.* **2018**, *8*, 1–8, doi:10.1038/s41598-018-31305-9.
24. Brant, J.A.; Labille, J.; Robichaud, C.O.; Wiesner, M. Fullerol cluster formation in aqueous solutions: Implications for environmental release. *J. Colloid Interface Sci.* **2007**, *314*, 281–288, doi:10.1016/j.jcis.2007.05.020.
25. Saraswati, T.E.; Setiawan, U.H.; Ihsan, M.R.; Isnaeni, I.; Herbani, Y. The Study of the Optical Properties of C60 Fullerene in Different Organic Solvents. *Open Chem.* **2020**, *17*, 1198–1212, doi:10.1515/chem-2019-0117.
26. Singh, R.; Goswami, T. Highly luminescent multifunctional hemi-ortho ester derivatives of fullerenol. *Synth. Met.* **2007**, *157*, 951–955, doi:10.1016/j.synthmet.2007.09.006.